

Model-independent Test of the Cosmic Anisotropy with Inverse Distance Ladder

Zong-Fan Yang¹, Da-Wei Yao², M. Le Delliou^{1,3,4,5,6,7}, and Ke Wang^{8*}

¹*School of Physical Science and Technology, Lanzhou University, Lanzhou 730000, China*

²*Beijing Zhihuo Technology Co., Ltd, Beijing 100000, China*

³*Institute of Theoretical Physics & Research Center of Gravitation, Lanzhou University, Lanzhou 730000, China*

⁴*Key Laboratory of Quantum Theory and Applications of MoE, Lanzhou University, Lanzhou 730000, China*

⁵*Lanzhou Center for Theoretical Physics & Key Laboratory of Theoretical Physics of Gansu Province, Lanzhou University, Lanzhou 730000, China*

⁶*Instituto de Astrofísica e Ciências do Espaço, Universidade de Lisboa,*

Faculdade de Ciências, Ed. C8, Campo Grande, 1769-016 Lisboa, Portugal

⁷*Université de Paris-Cité, APC-Astroparticule et Cosmologie (UMR-CNRS 7164), F-75006 Paris, France and*

⁸*Department of Physics, Liaoning Normal University, Dalian 116029, China*

(Dated: February 25, 2025)

If the Universe is endowed with cosmic anisotropy, it will have a preferred direction of expansion. Reconstructing the expansion history by Gaussian Process (GP) can be used to probe the cosmic anisotropy model-independently. In this paper, for the luminosity distance $d_L(z)$ reconstruction, we turn to the inverse distance ladder, where type Ia supernova (SNIa) from the Pantheon+ sample determine relative distances and strongly gravitationally lensed quasars from H0LiCOW sample anchor these relative distances with some absolute distance measurements. By isolating the anisotropic information that could be carried by the Hubble constant H_0 and obtaining constraints on the intrinsic parameter of SNIa, the absolute magnitude $M = -19.2522^{+0.0594}_{-0.0649}$ (at 68% CL), we find that $d_L(z)$ reconstructions from samples located in different region of the Galactic coordinate system are almost consistent with each other, while only a very weak preference for the cosmic anisotropy is found.

I. INTRODUCTION

The cosmological principle hypothesizes that the Universe features homogeneity and isotropy on large scales. Rooted on some basic important assumptions, including the cosmological principle, the standard model of particle physics and Einstein's theory of gravity, the standard model of cosmology is established. More precisely, according to the latest cosmic microwave background (CMB) observations [1], measurements of galaxy clustering and weak gravitational lensing [2] and measurements of baryon acoustic oscillation [3–5, BAO], the Lambda cold dark matter (Λ CDM) model is generally considered as being supported. Despite its successes on large cosmic scales, there are some underlying crises appearing on small scales, such as the presence of a dipole in the quasar [6–9], radio galaxy [10, 11] and active galactic nuclei sky [12], a smaller than predicted amplitude of matter fluctuations σ_8 obtained from cluster counts [13] and a larger local value of the Hubble constant H_0 [14] compared with CMB observations [1]. Besides modifying general relativity (GR), introducing dynamical dark energy models or different treatments of systematic uncertainty, these tensions also might be alleviated by departing from the cosmological principle. In particular, the 5.1σ tension between the number-count dipoles found jointly in the quasar and radio galaxy sky [10], and the CMB kinematic dipole [15], challenges the cosmological

principle directly. Therefore, it is imperative to know to what extent the cosmological principle is violated, hence the need for a further test of local cosmic inhomogeneity and anisotropy.

The most simple methods to test cosmic anisotropy are based on type Ia supernovae (SNIa) data, such as the Pantheon+ sample [16]. Since a large number of SNIa are spread out in the sky, one straightforward method is to divide the whole SNIa sample into several subsets according to its distribution. In particular, the hemisphere comparison method divides the whole sample into two data subsets and investigates the discrepancy between these two opposite hemispheres [17, 18]. To further probe the fine structure that might be smoothed out, one can use Hierarchical Equal Area iso-Latitude Pixelization [19, HEALPix] to divide the whole SNIa sample into several data subsets at a time. Another common method is the dipole fitting method, which assumes the observation of every SNIa depends on an *a priori* cosmic dipole [20]. The above three methods propose means of extracting cosmic anisotropy from SNIa data. However, most common methods further process the SNIa data in order to retrieve anisotropies in specific cosmological parameters, which in turn requires assuming a specific cosmological model. More precisely, the luminosity distance d_L is calculated in a specific cosmological model, such as in the Λ CDM model [21–25], w CDM model [26], CPL model [27], Finslerian model [28], or ALTB model [29]. However, the introduction of such model is not only not generic enough, but also source of potential biases.

If d_L can be calculated model-independently, one can make a model-independent test of the cosmic anisotropy

*Corresponding author: wangkey@lzu.edu.cn

with SNIa data. In fact, there are several ways to realize this ambition. For example, there are families of polynomials, function of redshift variables [30–32], or using the Padé approximation [33], in each case approximating d_L model-independently. Similarly, d_L can be expressed model-independently by the cosmographic parameters according to the well-known cosmographic approach [34, 35]. As for the completely data-driven non-parametric approach, d_L can be reconstructed model-independently by artificial neural network [36, ANN]. In some cases, one may only care about the relative distances from SNIa, where one can turn to Gaussian Process (GP) to reconstruct the dimensionless luminosity distance $D_L \equiv d_L H_0/c$ [37, 38]. In this paper, since we start from D_L , as GP proved useful to treat data model-independently, we will use GP to perform the reconstruction of D_L from the Pantheon+ sample [16].

Given the relative distances accessible from SNIa, one should anchor them with an absolute distance measurement. For the local distance ladder, H_0 and the absolute magnitude M of SNIa are usually calibrated by very local Cepheids [14, 16]. Although these very local absolute distance measurements are almost completely insensitive to the cosmological background model, they are too local to consider their spatial distribution, hence no anisotropic information can be extracted from them. On the contrary, the inverse distance ladder can be calibrated at high redshift using other independent measurements, such as the sound horizon at radiation drag r_d determined by CMB observations [39, 40], the time delays $\Delta t_{j,1}$ between the Refsdal Supernova’s j th and first appearances [41, 42], or the time-delay distance $d_{\Delta t}$ of strongly gravitationally lensed quasars [32, 43–47]. If anchors at high redshift are also spread out in the sky, they may carry certain anisotropic information, just as SNIa samples do. Therefore, in this paper, we will use $d_{\Delta t}$ measurements of six lensed quasars from the H0LiCOW sample [43] to anchor our D_L reconstructions from the Pantheon+ sample [16]. That is to say, we can model-independently test the cosmic relative or absolute anisotropy with D_L reconstructions only or the combination of D_L reconstructions and $d_{\Delta t}$ measurements respectively.

Should there exist cosmic anisotropy, the anisotropic information should affect all observations. Therefore a consistency test between different observations can further confirm the anisotropic information. On one hand, as the spatial separation between Cepheids restricts due to their small distances, they are not producing measurable anisotropy effects to cross-check with the Pantheon+ sample [16]. The H0LiCOW sample [43], on the other hand, consisting of objects located at higher redshifts, not only can serve as anchor of the inverse distance ladder, but also can carry the anisotropic information, which can then be cross-checked with the Pantheon+ sample. By choosing the inverse ladder anchor, we can extract anisotropies from the combined set of data, beyond the limits of SNIa data. As a result of the inverse ladder

approach, the consistency test in the latter part of our paper brings an advantage over the usual distance ladder. A successful test would reveal the presence of cosmic anisotropy in the entire data combination; a failed test proves that the anisotropy which appears in the Pantheon+ sample, but disappears in H0LiCOW sample, probably results from potential systematic uncertainties.

This paper is organized as follows. In section II, we introduce a model-independent method and the widespread data through the sky for $D_L(z)$ reconstruction, namely GP and the Pantheon+ sample [16]. Then, we present the anchors from the H0LiCOW sample [43] for the inverse distance ladder. In section III, we show the reconstruction of $d_L(z)$ from different datasets which serves as probe of the cosmic anisotropy in our paper. Finally, a brief summary and discussions are included in section IV.

II. METHODOLOGY AND DATA

In this section, we provide a brief summary of the model-independent GP algorithm, the SNIa data used for the Universe expansion history reconstruction and the strong gravitational lenses data used to anchor the inverse distance ladder.

A. Gaussian Process

While the Gaussian distribution describes the distribution of a random variable with mean and variance, GP describes the distribution of a function $f(x)$ with mean $\mu(x)$, variance $\sigma^2(x)$ and kernel $k(x, x')$. There are several choices of kernel function: squared exponential kernel, Matern (5/2) kernel, Matern (7/2) kernel or Matern (9/2) kernel, among others. Here we only use the squared exponential kernel

$$k(x, x') = \sigma_f^2 \exp \left[-\frac{(x - x')^2}{2l^2} \right], \quad (1)$$

where σ_f and l are the GP hyperparameters. The former determines the correlation strength between $f(x)$ and $f(x')$ at two different points, the latter gives the correlation length determining the range of such correlation.

Before reconstructing $f(x)$, these two hyperparameters should be known. Given the observed data $\{\mathbf{x}, \mathbf{y} = f(\mathbf{x}) \pm \sigma(\mathbf{x})\}$, σ_f and l can be determined by maximizing the marginal likelihood [38, 48]

$$\begin{aligned} \ln \mathcal{L} &= \ln P(\mathbf{y}|\mathbf{x}, \sigma_f, l) \\ &= -\frac{1}{2}(\mathbf{y} - \mu(\mathbf{x}))^T [k(\mathbf{x}, \mathbf{x}) + C]^{-1}(\mathbf{y} - \mu(\mathbf{x})) \\ &\quad - \frac{1}{2} \ln |k(\mathbf{x}, \mathbf{x}) + C| - \frac{n}{2} \ln 2\pi, \end{aligned} \quad (2)$$

where $C = C(\sigma(\mathbf{x}), \sigma(\mathbf{x}))$ is the covariance matrix of the data and n is the number of data points. After optimizing

for σ_f and l , $f(\mathbf{x})$ at points \mathbf{x}^* can be reconstructed as the mean of $f(\mathbf{x}^*)$

$$\overline{f(\mathbf{x}^*)} = \mu(\mathbf{x}^*) + k(\mathbf{x}^*, \mathbf{x})[k(\mathbf{x}, \mathbf{x}) + C]^{-1}(\mathbf{y} - \mu(\mathbf{x})) \quad (3)$$

with the covariance of $f(\mathbf{x}^*)$

$$\text{cov}(f(\mathbf{x}^*)) = k(\mathbf{x}^*, \mathbf{x}^*) - k(\mathbf{x}^*, \mathbf{x})[k(\mathbf{x}, \mathbf{x}) + C]^{-1}k(\mathbf{x}, \mathbf{x}^*). \quad (4)$$

Following the above procedures, we can reconstruct the cosmic expansion history by the GP package GaPP3 [38].

B. Pantheon+ sample

In this paper, we only use the Pantheon+ sample [16] to reconstruct $D_L(z)$. This dataset consists of 1701 light curves of 1550 distinct SNIa in the redshift range $0.001 < z < 2.26$. In Fig. 1, we show the distribution of these 1550 SNIa in the sky. Following the hemisphere comparison method [17, 18], we divide the full dataset into several subsets to probe cosmic anisotropy, as listed in Tab. I. Each SNIa subset provides information on a corresponding patch of the Universe.

Given the corrected apparent magnitudes m of SNIa, information about the luminosity distance d_L of SNIa can be derived from the relation between them as

$$\begin{aligned} m &= 5 \log_{10} \left[\frac{d_L}{1 \text{Mpc}} \right] + 25 + M \\ &= 5 \log_{10} \left[\frac{d_L H_0 / c}{1 \text{Mpc} \cdot H_0 / c} \right] + 25 + M \\ &= 5 \log_{10} [d_L H_0 / c] - 5 \log_{10} [10 \text{pc} \cdot H_0 / c] + M, \end{aligned} \quad (5)$$

where M is the absolute magnitude of SNIa. By defining a dimensionless luminosity distance $D_L \equiv d_L H_0 / c$ and a fiducial parameter $M_* \equiv M - 5 \log_{10} [10 \text{pc} \cdot H_0 / c]$, we have

$$D_L = 10^{\frac{m - M_*}{5}}. \quad (6)$$

It is worth noting that we, in fact, don't know the value of M_* . However we can express it as

$$\begin{aligned} M_* &= -19.3 + \delta_M - 5 \log_{10} [\delta_{70} \cdot 70 / (3 \times 10^{10})] \\ &= 23.86 + \delta_M - 5 \log_{10} [\delta_{70}], \end{aligned} \quad (7)$$

where $\delta_M - 19.3 = M$ and $\delta_{70} \cdot 70 \text{ km/s/Mpc} = H_0$ characterize the unknown information about M and H_0 . Since M is the intrinsic parameter of SNIa, δM (or M) should not be space-dependent or time-dependent when Newton's Constant G is supposed to be truly a constant, remaining unchanged [49–51]. By isolating the anisotropic information carried by δ_{70} (or H_0), we can determine δ_M from the following relation

$$\tilde{D}_L = D_L / \delta_{70} = d_L / c \cdot 70 \text{ km/s/Mpc} = 10^{\frac{m - 23.86 - \delta_M}{5}}. \quad (8)$$

If δ_M and δ_{70} are known, according to Eq. (6), we can obtain the covariance matrix of the \mathbf{D}_L vector of derived D_L s from the covariance matrix of the \mathbf{m} vector as

$$\mathbf{C}_{D_L} = \mathbf{J} \mathbf{C}_m \mathbf{J}^T, \quad (9)$$

where $J_{ii} = \frac{\partial D_{L,i}}{\partial m_i}$ is a diagonal Jacobian matrix. Then we can reconstruct $D_L(z)$ with the derived data $\{\mathbf{z}, \mathbf{D}_L, \mathbf{C}_{D_L}\}$ from the Pantheon+ sample [16]. Similarly, if only δ_M is known, according to Eq. (8), we can reconstruct $\tilde{D}_L(z)$ with the derived data $\{\mathbf{z}, \tilde{\mathbf{D}}_L, \mathbf{C}_{\tilde{D}_L}\}$ from the Pantheon+ sample [16].

C. H0LiCOW sample

The H0LiCOW sample consists of six lensed quasars [43], as listed in Tab. II. They also spread out in the sky, as shown in Fig. 1. For cosmological purposes, the effective time-delay distance $d_{\Delta t}$ of every lens system can be considered as derived data. Because we want to use $d_{\Delta t}$ measurements from the H0LiCOW sample [43] to anchor $D_L(z)$ (or $\tilde{D}_L(z)$) reconstructions at high redshifts, we need to convert the dimensionless luminosity distance reconstruction $D_L(z)$ into dimensionless angular diameter distance reconstruction $D_A(z) = D_L(z) / (1+z)^2$ and consequently into dimensionless time-delay distance of any lens system

$$D_{\Delta t} \equiv \frac{(1+z_l)D_A(z_l)(1+z_s)D_A(z_s)}{(1+z_s)D_A(z_s) - (1+z_l)D_A(z_l)} = d_{\Delta t} H_0 / c, \quad (10)$$

where z_l and z_s are the redshifts of lens and source respectively. To isolate the anisotropic information carried by H_0 , we turn to δ_{70} again

$$\tilde{D}_{\Delta t} = D_{\Delta t} / \delta_{70} = d_{\Delta t} / c \cdot 70 \text{ km/s/Mpc}. \quad (11)$$

III. RESULTS

In this section, we first determine the space-independent intrinsic parameters of SNIa, δ_M and M . Then we prove that the likelihood that we derive below in Eq. (15) does not depend on δ_{70} , nor on H_0 . Finally we obtain the space-dependent information from the reconstruction of $d_L(z)$ with known δ_M and M .

A. Determination of δ_M and M

Before testing cosmic anisotropy, we must have a good knowledge of the space-independent parameters, such as

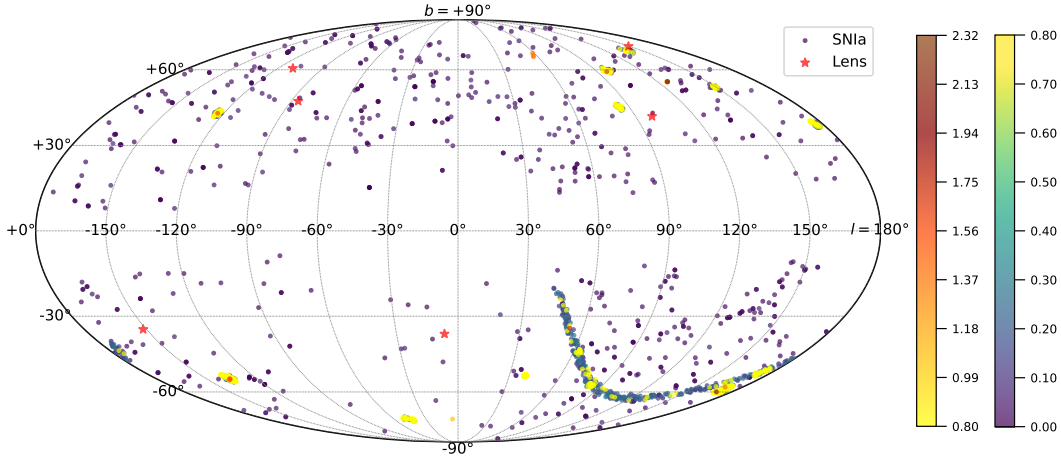


FIG. 1: Distribution of 1550 SNIa of the Pantheon+ sample [16] and 6 lenses of the H0LiCOW sample [43] in the Galactic coordinate system (l, b) , where the coloured dots represent SNIa with the two side bars indicating their redshifts and the red stars are lensed quasars.

TABLE I: Definitions of the full sky spatial divisions in the Galactic coordinate system (l, b) , resulting in corresponding subsamples from the distribution of 1550 SNIa of the Pantheon+ sample [16] and 6 lenses of the H0LiCOW sample [43]. The full dataset is divided into $\text{PH}_N + \text{PH}_S$ by a split along the Galactic plane, $\text{PH}_E + \text{PH}_W$ by a division along a plane orthogonal to the Galactic plane, $\text{PH}_{NE} + \text{PH}_{NW} + \text{PH}_{SE} + \text{PH}_{SW}$ by both simultaneous divisions and $\text{PH}_U + \text{PH}_D$ by a division along a plane orthogonal to the CMB dipole ($l = 264.02^\circ \pm 0.01^\circ, b = 48.25^\circ \pm 0.01^\circ$) [15].

Dataset	l	b	Size
PH_{All}	$-180^\circ \leq l < 180^\circ$	$-90^\circ \leq b \leq 90^\circ$	1701
PH_N	$-180^\circ \leq l < 180^\circ$	$0^\circ \leq b \leq 90^\circ$	664
PH_S	$-180^\circ \leq l < 180^\circ$	$-90^\circ \leq b < 0^\circ$	1037
PH_W	$-180^\circ \leq l < 0^\circ$	$-90^\circ \leq b \leq 90^\circ$	549
PH_E	$0^\circ \leq l < 180^\circ$	$-90^\circ \leq b \leq 90^\circ$	1152
PH_{NW}	$-180^\circ \leq l < 0^\circ$	$0^\circ \leq b \leq 90^\circ$	303
PH_{NE}	$0^\circ \leq l < 180^\circ$	$0^\circ \leq b \leq 90^\circ$	361
PH_{SW}	$-180^\circ \leq l < 0^\circ$	$-90^\circ \leq b < 0^\circ$	246
PH_{SE}	$0^\circ \leq l < 180^\circ$	$-90^\circ \leq b < 0^\circ$	791
PH_U	$(\cos b \cos l, \cos b \sin l, \sin b) \cdot (\cos 48.25 \cos 264.02, \cos 48.25 \sin 264.02, \sin 48.25) \geq 0$		634
PH_D	$(\cos b \cos l, \cos b \sin l, \sin b) \cdot (\cos 48.25 \cos 264.02, \cos 48.25 \sin 264.02, \sin 48.25) < 0$		1067

δ_M and M . From Eq. (11), the likelihood is

$$\begin{aligned} \mathcal{L} &= P(\tilde{\mathbf{D}}_{\Delta t}, \mathbf{d}_{\Delta t} | \delta_M, \mathcal{A}) \\ &= \exp \left[-\frac{1}{2} \left(\frac{c\tilde{\mathbf{D}}_{\Delta t}(\delta_M)/\mathbf{d}_{\Delta t}}{70 \text{ km/s/Mpc}} - 1 \right)^T \mathbf{C}_{\delta_M}^{-1} \right. \\ &\quad \left. \left(\frac{c\tilde{\mathbf{D}}_{\Delta t}(\delta_M)/\mathbf{d}_{\Delta t}}{70 \text{ km/s/Mpc}} - 1 \right) \right], \end{aligned} \quad (12)$$

where the prior assumption \mathcal{A} sets the mean value of $c\tilde{\mathbf{D}}_{\Delta t}/\mathbf{d}_{\Delta t}$ to 70 km/s/Mpc, the data vector $\tilde{\mathbf{D}}_{\Delta t}$ is derived from $\tilde{D}_L(z)$ given the redshift tensor (z_l, z_s) listed in Tab. II, the corresponding data vector $\mathbf{d}_{\Delta t}$ is given by

the H0LiCOW sample [43] directly and \mathbf{C}_{δ_M} is a diagonal matrix proportional to the variance of $\frac{P(\tilde{\mathbf{D}}_{\Delta t} | \delta_M)}{P(\mathbf{d}_{\Delta t})}$. We use the `emcee` [52] sampler to produce the Monte Carlo Markov Chain (MCMC) of δ_M with a uniform prior distribution over $(-0.3, 0.3)$. During the course of the calculation, each sample of the MCMC chain of δ_M is used to reconstruct $\tilde{D}_L(z)$ from the whole Pantheon+ sample [16] according to Eq. (8) by the GP package `GaPP3` [38]. Due to the prohibitive computational cost of $\tilde{D}_L(z)$ reconstructions with a large number of δ_M , we have to turn to the approximation of

$$\tilde{D}_L(z, \delta_M \neq 0) \approx \tilde{D}_L(z, \delta_M = 0) 10^{-\frac{\delta_M}{5}}. \quad (13)$$

TABLE II: Six lensed quasars of the H0LiCOW sample [43] in the Galactic coordinate system (l, b), where z_l and z_s are the redshifts of lens and source respectively.

Lens name	l	b	z_l	z_s
B1608 + 656	98.3397	40.8915	0.6304	1.394
RXJ1131 – 1231	-86.2504	46.8456	0.295	0.654
HE 0435 – 1223	-151.5704	-34.8188	0.4546	1.693
SDSS 1206 + 4332	148.9913	71.2445	0.745	1.789
WFI2033 – 4723	-6.6015	-36.5264	0.6575	1.662
PG 1115 + 080	-110.1126	60.6443	0.311	1.722

That is to say, we just reconstruct $\tilde{D}_L(z, \delta_M = 0)$ once. Then we obtain $\tilde{D}_L(z, \delta_M \neq 0)$ by adjusting the reconstruction of $\tilde{D}_L(z, \delta_M = 0)$ with $10^{-\frac{\delta_M}{5}}$, including its mean value and uncertainty. Finally, we get the posterior probability density function (PDF) of $\delta_M = 0.0478_{-0.0649}^{+0.0594}$ (at 68% CL), as shown in the left panel of Fig. 2. We also display the reconstruction of $\tilde{D}_L(z, \delta_M = 0.0478)$ in the right panel of Fig. 2. We find that $\delta_M > 0$ suppresses $\tilde{D}_L(z)$ and narrows its uncertainty, which agrees with the above approximation, Eq. (13).

B. Cancellation of δ_{70} and H_0

Given the space-independent parameter evaluation at $\delta_M = 0.0478_{-0.0649}^{+0.0594}$ (at 68% CL), we can rewrite Eq. (6) as

$$D_L = 10^{\frac{m-23.9078}{5}} \delta_{70}. \quad (14)$$

We then try to determine the space-dependent parameters, such as δ_{70} and H_0 . From Eq. (10), the likelihood is

$$\begin{aligned} \mathcal{L} &= P(\mathbf{D}_{\Delta t}, \mathbf{d}_{\Delta t} | \delta_{70}, \mathcal{A}) \\ &= \exp \left[-\frac{1}{2} \left(\frac{c\mathbf{D}_{\Delta t}(\delta_{70})/\mathbf{d}_{\Delta t}}{H_0} - 1 \right)^T \mathbf{C}_{\delta_{70}}^{-1} \right. \\ &\quad \left. \left(\frac{c\mathbf{D}_{\Delta t}(\delta_{70})/\mathbf{d}_{\Delta t}}{H_0} - 1 \right) \right], \quad (15) \end{aligned}$$

where the prior assumption \mathcal{A} sets the mean value of $c\mathbf{D}_{\Delta t}/\mathbf{d}_{\Delta t}$ to H_0 , the data vector $\mathbf{D}_{\Delta t}$ is derived from $D_L(z)$, given the redshift tensor $(\mathbf{z}_l, \mathbf{z}_s)$ listed in Tab. II, and the corresponding data vector $\mathbf{d}_{\Delta t}$ is given by the H0LiCOW sample [43] directly and $\mathbf{C}_{\delta_{70}}$ is a diagonal matrix proportional to the variance of $\frac{P(\mathbf{D}_{\Delta t} | \delta_{70})}{P(\mathbf{d}_{\Delta t})}$. When we turn to the approximation that

$$D_L(z, \delta_{70} \neq 1) \approx D_L(z, \delta_{70} = 1) \delta_{70}, \quad (16)$$

we just need to reconstruct $D_L(z, \delta_{70} = 1)$ once. Then we obtain $D_L(z, \delta_{70} \neq 1)$ by adjusting the reconstruction of $D_L(z, \delta_{70} = 1)$ with δ_{70} , including its mean value and

uncertainty. Consequently, δ_{70} cancels out from the prior assumption \mathcal{A} , as $c\mathbf{D}_{\Delta t}/\mathbf{d}_{\Delta t} = H_0$ therefore $c\mathbf{D}_{\Delta t}(\delta_{70} = 1)/\mathbf{d}_{\Delta t} = 70$ km/s/Mpc, which is independent from δ_{70} . That is to say, the likelihood Eq. (15) can not constrain δ_{70} , and thus H_0 .

C. Reconstruction of $d_L(z)$

Given the absolute magnitude evaluation $M = -19.3 + \delta_M = -19.2522_{-0.0649}^{+0.0594}$ (at 68% CL), we can reconstruct $d_L(z)$ from Eq. (5). To probe cosmic anisotropy, we compare reconstructions of $d_L(z)$ from every dataset listed in Tab. I, and display them, such as PH_N vs. PH_S , shown in the left panel of Fig. 3, PH_W vs. PH_E , shown in the left panel of Fig. 4, PH_{NW} vs. PH_{NE} vs. PH_{SW} vs. PH_{SE} , shown in the left panel of Fig. 5, or PH_U vs. PH_D , shown in the left panel of Fig. 6. We find that the $d_L(z)$ reconstructions from PH_N and PH_S are consistent with each other, as shown in the left panel of Fig. 3. Similarly, the $d_L(z)$ reconstructions from PH_W and PH_E , as well as from PH_U and PH_D , are also consistent with each other, as shown in the left panel of Fig. 4 and 6, respectively. However, the $d_L(z)$ reconstructions from PH_{NW} and PH_{SW} break consistency at higher redshift at 68% CL, as shown in the left panel of Fig. 5.

To further quantify the information about anisotropy carried by $d_L(z)$, we define

$$\delta_{i,\text{All}}(z) \equiv \frac{d_{L,i}(z) - \overline{d_{L,\text{All}}(z)}}{\overline{d_{L,\text{All}}(z)}}, \quad (17)$$

where $\overline{d_{L,\text{All}}(z)}$ is the mean value of the $d_L(z, \delta_M = 0.0478)$ reconstruction from the PH_{All} dataset (as plotted as the blue solid curve in the right panel of Fig. 2) and $d_{L,i}(z)$ is the reconstruction of $d_L(z, \delta_M = 0.0478)$ from the other datasets listed in Tab. I. We list the constraints on $\delta_{i,\text{All}}(z = 0.5)$, $\delta_{i,\text{All}}(z = 1.0)$, $\delta_{i,\text{All}}(z = 1.5)$ and $\delta_{i,\text{All}}(z = 2.0)$ at 68% CL. in Tab. III. We find that $\delta_{\text{NW},\text{All}}(z = 2.0) = -0.2412 \pm 0.1498$ (at 68% CL) and $\delta_{\text{SW},\text{All}}(z = 2.0) = 0.0515 \pm 0.0914$ (at 68% CL) are mutually inconsistent. This inconsistency of more than 1σ can be regarded as a weak preference for cosmic anisotropy. However, as the $d_L(z)$ reconstruction is model independent, it takes into account any possible source of anisotropy, including the Hubble parameter $H(z)$ or cosmic curvature Ω_k . The anisotropy effect can be expressed in $d_L(z) = d_L(z, H(z), \Omega_k)$ even though there is no specific cosmological model assumed. Therefore, we can not disentangle the cosmic anisotropy source between Hubble expansion and cosmic curvature.

In fact, the above inconsistency between $d_L(z)$ from the PH_W and PH_E datasets can either be regarded as anisotropic information from the Pantheon+ sample [16] or as inconsistency in SNIa data from potential systematic uncertainties. Undoubtedly, if the above inconsistency do result from cosmic anisotropy, the anisotropic information should affect both the Pantheon+ sample [16] and the H0LiCOW sample [43]. We therefore

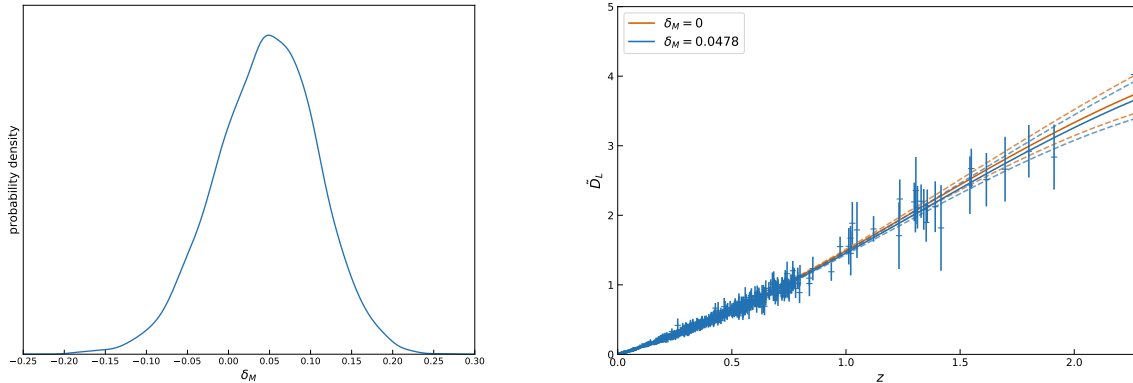


FIG. 2: LEFT: Posterior PDF of δ_M . RIGHT: Reconstruction of $\tilde{D}_L(z, \delta_M = 0)$ (red curve, $\sigma_f = 3.0579$, $l = 2.4832$) and $\tilde{D}_L(z, \delta_M = 0.0478)$ (blue curve, $\sigma_f = 2.9913$, $l = 2.4832$) from the whole Pantheon+ sample [16], blue points with errorbars for the $\delta_M = 0.0478$ reconstruction, according to Eq. (8) by the GP package `GaPP3` [38], where the bracketing dashed curves define the 68% CL regions of the reconstructions.

TABLE III: Constraints on $\delta_{i,\text{All}}(z = 0.5)$, $\delta_{i,\text{All}}(z = 1.0)$, $\delta_{i,\text{All}}(z = 1.5)$ and $\delta_{i,\text{All}}(z = 2.0)$ at 68% CL.

$\delta_{i,\text{All}}(z)$	$z = 0.5$	$z = 1.0$	$z = 1.5$	$z = 2.0$
$\delta_{\text{N,All}}(z)$	0.0049 ± 0.0096	0.0008 ± 0.0203	-0.0130 ± 0.0412	-0.0338 ± 0.0709
$\delta_{\text{S,All}}(z)$	-0.0032 ± 0.0075	-0.0016 ± 0.0187	0.0024 ± 0.0414	0.0049 ± 0.0744
$\delta_{\text{W,All}}(z)$	-0.0005 ± 0.0099	0.0065 ± 0.0229	0.0155 ± 0.0493	0.0238 ± 0.0871
$\delta_{\text{E,All}}(z)$	0.0003 ± 0.0073	-0.0055 ± 0.0174	-0.0229 ± 0.0366	-0.0481 ± 0.0644
$\delta_{\text{NW,All}}(z)$	0.0144 ± 0.0163	-0.0269 ± 0.0454	-0.1172 ± 0.0948	-0.2412 ± 0.1498
$\delta_{\text{NE,All}}(z)$	0.0021 ± 0.0114	0.0001 ± 0.0228	-0.0185 ± 0.0442	-0.0485 ± 0.0750
$\delta_{\text{SW,All}}(z)$	-0.0101 ± 0.0124	-0.0003 ± 0.0263	0.0220 ± 0.0524	0.0515 ± 0.0914
$\delta_{\text{SE,All}}(z)$	-0.0016 ± 0.0091	-0.0194 ± 0.0256	-0.0588 ± 0.0561	-0.1181 ± 0.0959
$\delta_{\text{U,All}}(z)$	0.0052 ± 0.0096	0.0007 ± 0.0204	-0.0139 ± 0.0413	-0.0354 ± 0.0713
$\delta_{\text{D,All}}(z)$	-0.0027 ± 0.0075	-0.0016 ± 0.0188	-0.0008 ± 0.0417	-0.0041 ± 0.0746

also need to check whether this anisotropic information is present in the H0LiCOW sample [43]. Here, we use the prediction of $d_{\Delta t}$ from different dataset to test their consistency and probe the impact of potential systematic uncertainties. Firstly, we define the average derived-to-measured effective time-delay distance

$$I \equiv \frac{1}{N} \sum_{i=1}^N \frac{d_{\Delta t,i}^P}{d_{\Delta t,i}^H}, \quad (18)$$

where $d_{\Delta t,i}^H$ is the measured effective time-delay distance of the H0LiCOW i -th lens system listed in Tab. I and $d_{\Delta t,i}^P$ is that derived from the partial Pantheon+ sample restricted to the same dataset, using Eq. (10). We compare the constraints on I from every dataset listed in Tab. I, and represent them separately: PH_N vs. PH_S is shown in Fig. 3, right panel, PH_W vs. PH_E in Fig. 4's right panel, PH_NW vs. PH_NE vs. PH_SW is portrayed in Fig. 5's right panel, while PH_U vs. PH_D is displayed in Fig. 6's right panel. We also list the constraints on I at 68% CL in Tab. IV. We find that the tested I s are con-

sistent pairwise: PH_N and PH_S ; PH_W and PH_E ; PH_NE and PH_SW ; PH_U and PH_D ; they are all consistent with $I = 1$, marking agreement between H0LiCOW and Pantheon+ data. Although the pairs of samples from PH_U and PH_N on one hand, and from PH_D and PH_S on another hand, contain populations of SNIa with different sizes, they include the same lensed systems. The values for $\delta_{\text{U,All}}(z)$ and $\delta_{\text{D,All}}(z)$ are both consistent with 0 and their I s are also consistent with each other, which mark no detectable difference between these two hemispheres in effective time-delay distance or luminosity distance, parallel to the CMB dipole. Note that as there is no lensed quasar in the PH_SE dataset, there is no constraint on I from a $d_{\Delta t,i}^H$ for this dataset. However, we obtain $I = 1.1051_{-0.0813}^{+0.1427}$ (at 68% CL) from PH_NW , which deviates at more than 1σ from $I = 1$. Thus, the prediction from the partial Pantheon+ sample is not consistent with the corresponding lensed system measurements for PH_NW , which means that the PH_NW dataset cannot be considered self-consistent. Therefore, we cannot guarantee that the reconstruction inconsistencies in $d_L(z)$ be-

TABLE IV: Constraints on I at 68% CL. Since there is no $d_{\Delta t, i}^H$ in the PH_{SE} dataset, there is no constraint on I .

Dataset	I
PH _N	$1.0279^{+0.0974}_{-0.1030}$
PH _S	$0.9583^{+0.0789}_{-0.0774}$
PH _W	$1.0068^{+0.0882}_{-0.0989}$
PH _E	$0.9783^{+0.1093}_{-0.0844}$
PH _{NW}	$1.1051^{+0.1427}_{-0.0813}$
PH _{NE}	$0.9820^{+0.1232}_{-0.0923}$
PH _{SW}	$0.9273^{+0.0826}_{-0.0787}$
PH _{SE}	–
PH _U	$1.0289^{+0.0975}_{-0.1027}$
PH _D	$0.9630^{+0.0804}_{-0.0773}$

tween PH_{NW} and PH_{SW} result from cosmic anisotropy rather than SNIa data systematics.

IV. SUMMARY AND DISCUSSION

In this paper, we reconstruct the luminosity distance $d_L(z)$ model-independently from different spatially selected datasets to probe cosmic anisotropy. We start with no prior knowledge of M , the absolute magnitude of SNIas, into which H_0 is degenerate. We eliminate that degeneracy by focusing on the reconstruction of $\tilde{D}_L(z)$, the dimensionless luminosity distance at a fiducial H_0 that only depends on M through a parameter δ_M in Eq. (8), from the whole Pantheon+ sample [16]. In addition, anchoring the $\tilde{D}_L(z)$ reconstruction with the H0LiCOW sample [43], we can extract a measurement of M as $M = -19.2522^{+0.0594}_{-0.0649}$ (at 68% CL). We finally reintroduce H_0 and Ω_k , the unknown value of the curvature parameter, into a model-independent reconstruction of $d_L(z)$ from the different datasets listed in Tab. I, using Eq. (5). We find that our reconstructions of $d_L(z)$ from these datasets, covering the complete Pantheon+ sample, show consistency between most of the subsamples, as shown in the left panel of Fig. 3, Fig. 4, Fig. 5 and Fig. 6, except between PH_{NW} and PH_{SW}, at higher redshift (at 68% CL), as shown in the left panel of Fig. 5. Our results are consistent with those of [25, 33]. The low (resp. high) redshift predictions listed in Tab. III for $d_L(z = 0.5)$ (resp. $d_L(z = 2.0)$) from PH_{SW} are smaller (resp. larger) than their counterparts from the other subsets. This is in agreement with the [25, 33] detections of a maximum H_0 and a minimum Ω_m in the ($l \sim 310^\circ, b \sim -15^\circ$) direction of the SNIa sky, as it corresponds to an anisotropy in the SW sky of our division and follows the low (resp. high) redshift relation

between luminosity distance and H_0 (resp. Ω_m). After a further consistency test comparing the Pantheon+ and H0LiCOW samples, we find that the PH_{NW} dataset is not self-consistent. Therefore, cosmic anisotropy is just one possible source for the above mentioned more than 1σ level inconsistency between PH_{NW} and PH_{SW}.

The method applied in our paper can not constrain some important cosmological parameters, such as H_0 or Ω_k . While they can carry anisotropic information and the constraints on H_0 can help deal with the Hubble tension, direct reconstruction of $d_L(z)$ is unable to distinguish, in the end, between Hubble parameter and curvature sources of anisotropy. Of course, direct reconstruction of $H(z)$ retains merit on its own, such as giving constraints on H_0 or Ω_k as was done in [44]. However, since our method departs from the fiducial relation $M_* = -19.3 - 5 \log_{10}[70/(3 \times 10^{10})]$, the presence of two new parameters δ_M and δ_{70} makes direct reconstruction of $H(z)$ impossible. Should one insist in constraining cosmological parameters, one can either turn to the reconstruction of $d_L(z) \approx \frac{cz}{H_0}$ at lower redshift, that only allows to circumscribe H_0 from SNIa with lower redshifts, or to the reconstruction of $d_L(z) = \frac{c(1+z)}{H_0} \int_0^z \frac{dz'}{(\Omega_m(1+z')^3 + \Omega_\Lambda)^{1/2}}$ at higher redshift, to constrain $\{H_0, \Omega_m, \Omega_\Lambda\}$ in the Λ CDM model. In other words, our model-independent method is more general and powerful than the methods from [21–29] and our results can be applied to any cosmological models.

Although our paper is only using six lensed quasars from H0LiCOW, they constitute a large enough sample to serve as good anchors. More precisely, according to Eq. (12), each lensed system’s effective time-delay distance $d_{\Delta t}$ is combined to anchor δ_M . Of course, the number of lensed system may affects the constraints on δ_M . As hinted in the right panel of Fig. 2, however, the method’s shifted mean value of $\delta_M \neq 0.0478$ (or $M \neq 19.2522$) used in the reconstruction of $d_L(z)$ according to Eq. (5) just shifts the results shown in the left panel of Fig. 3, Fig. 4, Fig. 5 and Fig. 6 but does not change their consistency. Therefore, the lensed sample size is less important than the consistency between them and SNIa data, which is what we have checked in Eq. (18).

Acknowledgments

MLeD acknowledges the financial support by the Lanzhou University starting fund, the Fundamental Research Funds for the Central Universities (Grant No. lzujbky-2019-25) and NSFC (grant No.12247101).

[1] N. Aghanim *et al.* [Planck], “Planck 2018 results. VI. Cosmological parameters,” *Astron. Astrophys.* **641**, A6

(2020) [erratum: *Astron. Astrophys.* **652**, C4 (2021)]

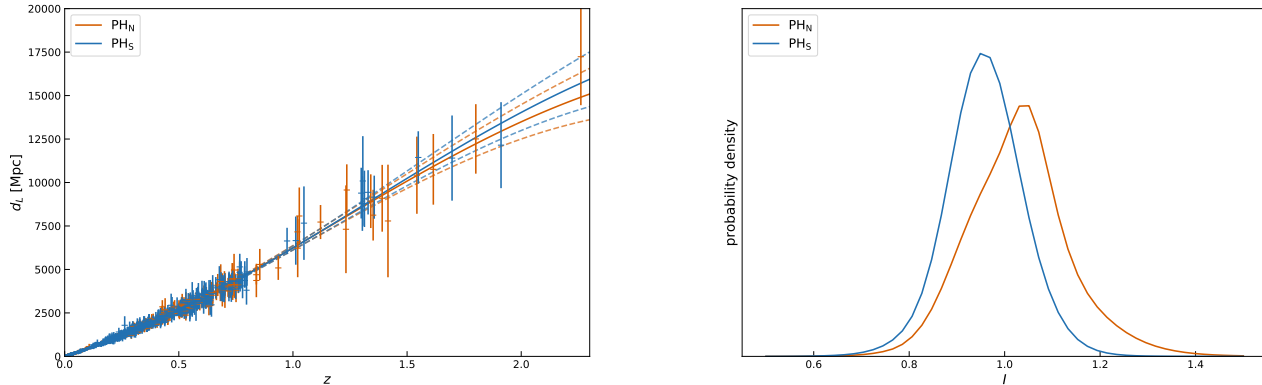


FIG. 3: LEFT: Reconstruction of $d_L(z, \delta_M = 0.0478)$ from the PH_N and PH_S datasets (red, $\sigma_f = 1.1322 \times 10^4$ Mpc, $l = 2.2562$, and blue, $\sigma_f = 1.2099 \times 10^4$ Mpc, $l = 2.3741$, resp.), where the bracketing dashed curves define the 68% CL regions of the reconstructions. RIGHT: Constraints on I from the PH_N and PH_S datasets (red and blue, resp.).

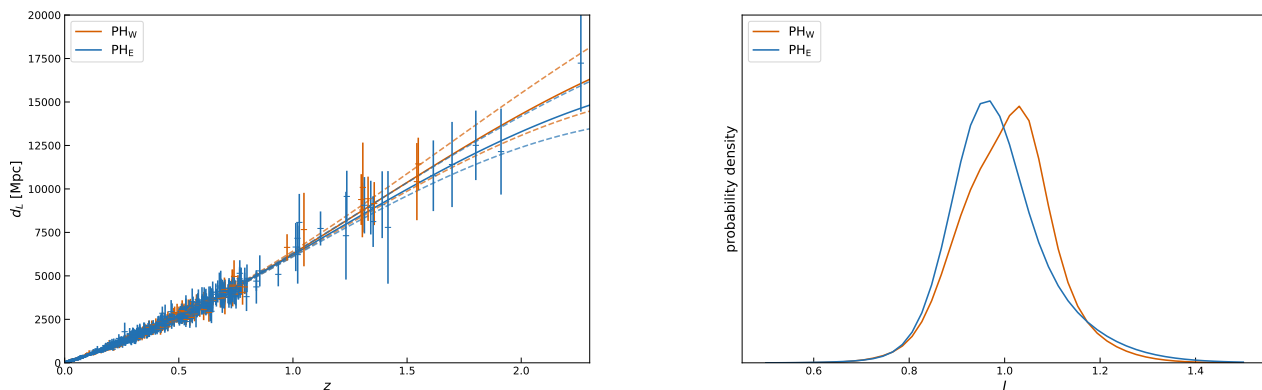


FIG. 4: LEFT: Reconstruction of $d_L(z, \delta_M = 0.0478)$ from the PH_W and PH_E datasets (red, $\sigma_f = 1.2782 \times 10^4$ Mpc, $l = 2.4030$, and blue, $\sigma_f = 1.1363 \times 10^4$ Mpc, $l = 2.2433$, resp.), where the bracketing dashed curves define the 68% CL regions of the reconstructions. RIGHT: Constraints on I from the PH_W and PH_E datasets (red and blue, resp.).

- [arXiv:1807.06209 [astro-ph.CO]].
- [2] T. M. C. Abbott *et al.* [DES], “Dark Energy Survey Year 3 results: Cosmological constraints from galaxy clustering and weak lensing,” *Phys. Rev. D* **105**, no.2, 023520 (2022) [arXiv:2105.13549 [astro-ph.CO]].
- [3] T. M. C. Abbott *et al.* [DES], “Dark Energy Survey: A 2.1% Measurement of the Angular Baryonic Acoustic Oscillation Scale at Redshift $z_{\text{eff}}=0.85$ from the Final Dataset,” [arXiv:2402.10696 [astro-ph.CO]].
- [4] S. Alam *et al.* [eBOSS], “Completed SDSS-IV extended Baryon Oscillation Spectroscopic Survey: Cosmological implications from two decades of spectroscopic surveys at the Apache Point Observatory,” *Phys. Rev. D* **103**, no.8, 083533 (2021) [arXiv:2007.08991 [astro-ph.CO]].
- [5] A. G. Adame *et al.* [DESI], “DESI 2024 VI: Cosmological

- Constraints from the Measurements of Baryon Acoustic Oscillations,” [arXiv:2404.03002 [astro-ph.CO]].
- [6] N. J. Secrest, S. von Hausegger, M. Rameez, R. Mohayaee, S. Sarkar and J. Colin, “A Test of the Cosmological Principle with Quasars,” *Astrophys. J. Lett.* **908**, no.2, L51 (2021) [arXiv:2009.14826 [astro-ph.CO]].
- [7] L. Dam, G. F. Lewis and B. J. Brewer, “Testing the cosmological principle with CatWISE quasars: a bayesian analysis of the number-count dipole,” *Mon. Not. Roy. Astron. Soc.* **525**, no.1, 231-245 (2023) [arXiv:2212.07733 [astro-ph.CO]].
- [8] R. Kothari, M. Panwar, G. Singh, P. Tiwari and P. Jain, “A study of dipolar signal in distant Quasars with various observables,” *Eur. Phys. J. C* **84**, no.1, 75 (2024) [arXiv:2208.14397 [astro-ph.CO]].

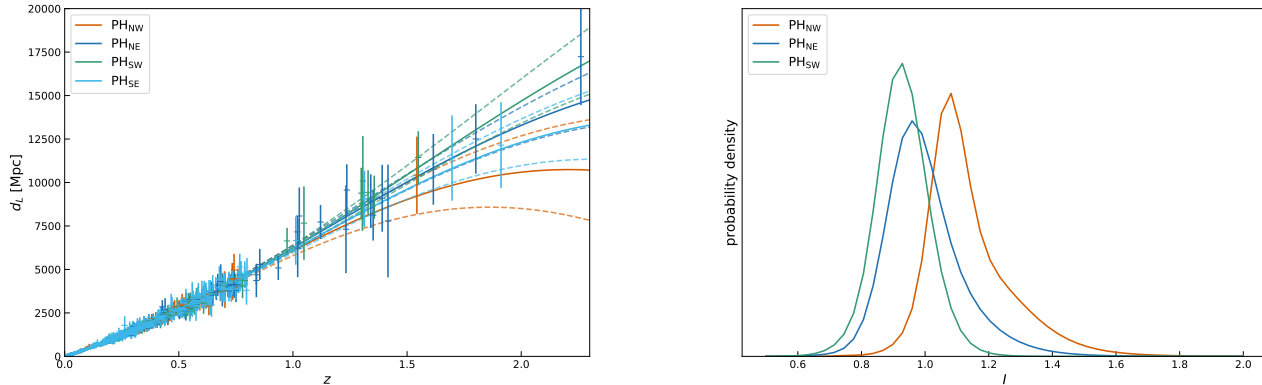


FIG. 5: LEFT: Reconstruction of $d_L(z, \delta_M = 0.0478)$ from the PH_{NW} , PH_{NE} , PH_{SW} and PH_{SE} datasets (red, $\sigma_f = 7.1685 \times 10^3$ Mpc, $l = 1.6094$, blue, $\sigma_f = 1.1006 \times 10^4$ Mpc, $l = 2.1561$, green, $\sigma_f = 1.4135 \times 10^4$ Mpc, $l = 2.5138$, and cyan, $\sigma_f = 8.8715 \times 10^3$ Mpc, $l = 1.9486$, resp.), where the bracketing dashed curves define the 68% CL regions of the reconstructions. RIGHT: Constraints on I from the PH_{NW} , PH_{NE} and PH_{SW} datasets (red, blue and green, resp.). Since there is no $d_{\Delta t, i}^H$ in the PH_{SE} dataset, there is no constraint on I from it.

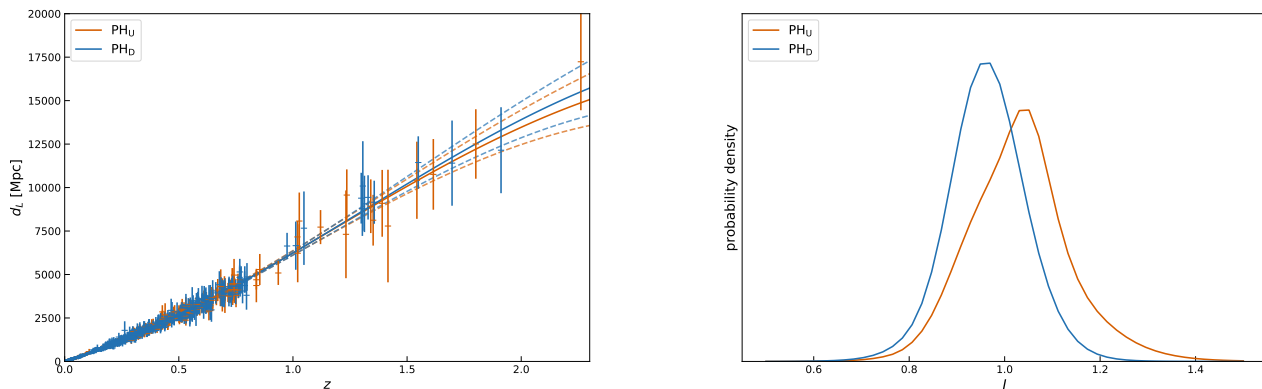


FIG. 6: LEFT: Reconstruction of $d_L(z, \delta_M = 0.0478)$ from the PH_{U} and PH_{D} datasets (red, $\sigma_f = 1.1696 \times 10^4$ Mpc, $l = 2.2704$, and blue, $\sigma_f = 1.1314 \times 10^4$ Mpc, $l = 2.3005$, resp.), where the the 68% CL regions of the reconstructions. RIGHT: Constraints on I from the PH_{U} and PH_{D} datasets (red and blue, resp.).

- [9] M. Panwar, P. Jain and A. Omar, “Colour dependence of dipole in CatWISE2020 data,” *Mon. Not. Roy. Astron. Soc.* **535**, no.1, L63-L69 (2024) [arXiv:2405.16853 [astro-ph.CO]].
- [10] N. J. Secrest, S. von Hausegger, M. Rameez, R. Mohayae and S. Sarkar, “A Challenge to the Standard Cosmological Model,” *Astrophys. J. Lett.* **937**, no.2, L31 (2022) [arXiv:2206.05624 [astro-ph.CO]].
- [11] J. D. Wagenveld, H. R. Klöckner and D. J. Schwarz, “The cosmic radio dipole: Bayesian estimators on new and old radio surveys,” *Astron. Astrophys.* **675**, A72 (2023) [arXiv:2305.15335 [astro-ph.CO]].
- [12] A. K. Singal, “Cosmic dipoles of active galactic nuclei at

- optical and radio wavelengths display much larger amplitudes than the cosmic microwave background dipole,” *Mon. Not. Roy. Astron. Soc.* **532**, no.1, L1-L6 (2024) [arXiv:2403.16581 [astro-ph.CO]].
- [13] P. A. R. Ade *et al.* [Planck], “Planck 2015 results. XXIV. Cosmology from Sunyaev-Zeldovich cluster counts,” *Astron. Astrophys.* **594**, A24 (2016) [arXiv:1502.01597 [astro-ph.CO]].
- [14] A. G. Riess, W. Yuan, L. M. Macri, D. Scolnic, D. Brout, S. Casertano, D. O. Jones, Y. Murakami, L. Breuval and T. G. Brink, *et al.* “A Comprehensive Measurement of the Local Value of the Hubble Constant with $1 \text{ km s}^{-1} \text{ Mpc}^{-1}$ Uncertainty from the Hubble Space Telescope

- and the SH0ES Team,” *Astrophys. J. Lett.* **934**, no.1, L7 (2022) [arXiv:2112.04510 [astro-ph.CO]].
- [15] N. Aghanim *et al.* [Planck], “Planck 2018 results. I. Overview and the cosmological legacy of Planck,” *Astron. Astrophys.* **641**, A1 (2020) [arXiv:1807.06205 [astro-ph.CO]].
- [16] D. Brout, D. Scolnic, B. Popovic, A. G. Riess, J. Zuntz, R. Kessler, A. Carr, T. M. Davis, S. Hinton and D. Jones, *et al.* “The Pantheon+ Analysis: Cosmological Constraints,” *Astrophys. J.* **938**, no.2, 110 (2022) [arXiv:2202.04077 [astro-ph.CO]].
- [17] D. J. Schwarz and B. Weinhorst, “(An)isotropy of the Hubble diagram: Comparing hemispheres,” *Astron. Astrophys.* **474**, 717-729 (2007) [arXiv:0706.0165 [astro-ph]].
- [18] I. Antoniou and L. Perivolaropoulos, “Searching for a Cosmological Preferred Axis: Union2 Data Analysis and Comparison with Other Probes,” *JCAP* **12**, 012 (2010) [arXiv:1007.4347 [astro-ph.CO]].
- [19] K. M. Górski, E. Hivon, A. J. Banday, B. D. Wandelt, F. K. Hansen, M. Reinecke and M. Bartelman, “HEALPix - A Framework for high resolution discretization, and fast analysis of data distributed on the sphere,” *Astrophys. J.* **622**, 759-771 (2005) [arXiv:astro-ph/0409513 [astro-ph]].
- [20] A. Mariano and L. Perivolaropoulos, “Is there correlation between Fine Structure and Dark Energy Cosmic Dipoles?,” *Phys. Rev. D* **86**, 083517 (2012) [arXiv:1206.4055 [astro-ph.CO]].
- [21] H. K. Deng and H. Wei, “Testing the Cosmic Anisotropy with Supernovae Data: Hemisphere Comparison and Dipole Fitting,” *Phys. Rev. D* **97**, no.12, 123515 (2018) doi:10.1103/PhysRevD.97.123515 [arXiv:1804.03087 [astro-ph.CO]].
- [22] Z. Q. Sun and F. Y. Wang, “Testing the anisotropy of cosmic acceleration from Pantheon supernovae sample,” *Mon. Not. Roy. Astron. Soc.* **478**, no.4, 5153-5158 (2018) [arXiv:1805.09195 [astro-ph.CO]].
- [23] H. K. Deng and H. Wei, “Null signal for the cosmic anisotropy in the Pantheon supernovae data,” *Eur. Phys. J. C* **78**, no.9, 755 (2018) [arXiv:1806.02773 [astro-ph.CO]].
- [24] D. Zhao, Y. Zhou and Z. Chang, “Anisotropy of the Universe via the Pantheon supernovae sample revisited,” *Mon. Not. Roy. Astron. Soc.* **486**, no.4, 5679-5689 (2019) [arXiv:1903.12401 [astro-ph.CO]].
- [25] J. P. Hu, Y. Y. Wang, J. Hu and F. Y. Wang, “Testing the cosmological principle with the Pantheon+ sample and the region-fitting method,” *Astron. Astrophys.* **681**, A88 (2024) [arXiv:2310.11727 [astro-ph.CO]].
- [26] W. Zhao, P. X. Wu and Y. Zhang, “Anisotropy of Cosmic Acceleration,” *Int. J. Mod. Phys. D* **22**, 1350060 (2013) [arXiv:1305.2701 [astro-ph.CO]].
- [27] H. N. Lin, S. Wang, Z. Chang and X. Li, “Testing the isotropy of the Universe by using the JLA compilation of type-Ia supernovae,” *Mon. Not. Roy. Astron. Soc.* **456**, no.2, 1881-1885 (2016) [arXiv:1504.03428 [astro-ph.CO]].
- [28] Z. Chang, D. Zhao and Y. Zhou, “Constraining the anisotropy of the Universe with the Pantheon supernovae sample,” *Chin. Phys. C* **43**, no.12, 125102 (2019) [arXiv:1910.06883 [astro-ph.CO]].
- [29] K. Wang, K. P. Chen and M. Le Delliou, “Constraints on the local cosmic void from the Pantheon supernovae data,” *Eur. Phys. J. C* **83**, no.9, 859 (2023) [arXiv:2304.13945 [astro-ph.CO]].
- [30] İ. Semiz and A. K. Çamlıbel, “What do the cosmological supernova data really tell us?,” *JCAP* **12**, 038 (2015) [arXiv:1505.04043 [gr-qc]].
- [31] A. K. Çamlıbel, İ. Semiz and M. A. Feyizoğlu, “Pantheon update on a model-independent analysis of cosmological supernova data,” *Class. Quant. Grav.* **37**, no.23, 235001 (2020) doi:10.1088/1361-6382/abba48 [arXiv:2001.04408 [astro-ph.CO]].
- [32] T. Collett, F. Montanari and S. Rasanen, “Model-Independent Determination of H_0 and Ω_{K0} from Strong Lensing and Type Ia Supernovae,” *Phys. Rev. Lett.* **123**, no.23, 231101 (2019) [arXiv:1905.09781 [astro-ph.CO]].
- [33] J. Hu, J. Hu, X. Jia, B. Gao and F. Wang, “Testing cosmic anisotropy with Padé approximations and the latest Pantheon+ sample,” *Astron. Astrophys.* **689**, A215 (2024) [arXiv:2406.14827 [astro-ph.CO]].
- [34] U. Andrade, C. A. P. Bengaly, B. Santos and J. S. Alcaniz, “A Model-independent Test of Cosmic Isotropy with Low- z Pantheon Supernovae,” *Astrophys. J.* **865**, no.2, 119 (2018) [arXiv:1806.06990 [astro-ph.CO]].
- [35] C. Cattoen and M. Visser, “Cosmography: Extracting the Hubble series from the supernova data,” [arXiv:gr-qc/0703122 [gr-qc]].
- [36] G. J. Wang, X. J. Ma, S. Y. Li and J. Q. Xia, “Reconstructing Functions and Estimating Parameters with Artificial Neural Networks: A Test with a Hubble Parameter and SNe Ia,” *Astrophys. J. Suppl.* **246**, no.1, 13 (2020) [arXiv:1910.03636 [astro-ph.CO]].
- [37] J. F. Jesus, R. Valentim, A. A. Escobal and S. H. Pereira, “Gaussian Process Estimation of Transition Redshift,” *JCAP* **04**, 053 (2020) [arXiv:1909.00090 [astro-ph.CO]].
- [38] M. Seikel, C. Clarkson and M. Smith, “Reconstruction of dark energy and expansion dynamics using Gaussian processes,” *JCAP* **06**, 036 (2012) [arXiv:1204.2832 [astro-ph.CO]].
- [39] É. Aubourg *et al.* [BOSS], “Cosmological implications of baryon acoustic oscillation measurements,” *Phys. Rev. D* **92**, no.12, 123516 (2015) [arXiv:1411.1074 [astro-ph.CO]].
- [40] A. J. Cuesta, L. Verde, A. Riess and R. Jimenez, “Calibrating the cosmic distance scale ladder: the role of the sound horizon scale and the local expansion rate as distance anchors,” *Mon. Not. Roy. Astron. Soc.* **448**, no.4, 3463-3471 (2015) [arXiv:1411.1094 [astro-ph.CO]].
- [41] P. L. Kelly, S. Rodney, T. Treu, M. Oguri, W. Chen, A. Zitrin, S. Birrer, V. Bonvin, L. Dessart and J. M. Diego, *et al.* “Constraints on the Hubble constant from supernova Refsdal’s reappearance,” *Science* **380**, no.6649, abh1322 (2023) [arXiv:2305.06367 [astro-ph.CO]].
- [42] X. Li and K. Liao, “Determining Cosmological-model-independent H_0 with Gravitationally Lensed Supernova Refsdal,” *Astrophys. J.* **966**, no.1, 121 (2024) [arXiv:2401.12052 [astro-ph.CO]].
- [43] K. C. Wong, S. H. Suyu, G. C. F. Chen, C. E. Rusu, M. Millon, D. Sluse, V. Bonvin, C. D. Fassnacht, S. Taubenberger and M. W. Auger, *et al.* “HOLiCOW – XIII. A 2.4 per cent measurement of H_0 from lensed quasars: 5.3σ tension between early- and late-Universe probes,” *Mon. Not. Roy. Astron. Soc.* **498**, no.1, 1420-1439 (2020) [arXiv:1907.04869 [astro-ph.CO]].
- [44] K. Liao, A. Shafieloo, R. E. Keeley and E. V. Linder,

- “A model-independent determination of the Hubble constant from lensed quasars and supernovae using Gaussian process regression,” *Astrophys. J. Lett.* **886**, no.1, L23 (2019) [arXiv:1908.04967 [astro-ph.CO]].
- [45] S. Taubenberger, S. H. Suyu, E. Komatsu, I. Jee, S. Birrer, V. Bonvin, F. Courbin, C. E. Rusu, A. J. Shajib and K. C. Wong, “The Hubble Constant determined through an inverse distance ladder including quasar time delays and Type Ia supernovae,” *Astron. Astrophys.* **628**, L7 (2019) [arXiv:1905.12496 [astro-ph.CO]].
- [46] K. Liao, A. Shafieloo, R. E. Keeley and E. V. Linder, “Determining Model-independent H_0 and Consistency Tests,” *Astrophys. J. Lett.* **895**, no.2, L29 (2020) [arXiv:2002.10605 [astro-ph.CO]].
- [47] X. Li, R. E. Keeley, A. Shafieloo and K. Liao, “A Model-independent Method to Determine H_0 Using Time-delay Lensing, Quasars, and Type Ia Supernovae,” *Astrophys. J.* **960**, no.2, 103 (2024) [arXiv:2308.06951 [astro-ph.CO]].
- [48] A. Shafieloo, A. G. Kim and E. V. Linder, “Gaussian Process Cosmography,” *Phys. Rev. D* **85**, 123530 (2012) [arXiv:1204.2272 [astro-ph.CO]].
- [49] W. Zhao, B. S. Wright and B. Li, “Constraining the time variation of Newton’s constant G with gravitational-wave standard sirens and supernovae,” *JCAP* **10**, 052 (2018) [arXiv:1804.03066 [astro-ph.CO]].
- [50] K. Wang and L. Chen, “Constraints on Newton’s constant from cosmological observations,” *Eur. Phys. J. C* **80**, no.6, 570 (2020) [arXiv:2004.13976 [astro-ph.CO]].
- [51] Y. Liu, H. Yu and P. Wu, “Alleviating the Hubble-constant tension and the growth tension via a transition of absolute magnitude favored by the Pantheon+ sample,” *Phys. Rev. D* **110**, no.2, L021304 (2024) [arXiv:2406.02956 [astro-ph.CO]].
- [52] D. Foreman-Mackey, D. W. Hogg, D. Lang and J. Goodman, “emcee: The MCMC Hammer,” *Publ. Astron. Soc. Pac.* **125**, 306-312 (2013) [arXiv:1202.3665 [astro-ph.IM]].